Overcoming phonon-induced dephasing for indistinguishable photon sources

2012 New J. Phys. 14 113004

(http://iopscience.iop.org/1367-2630/14/11/113004)

New Journal of Physics
The open access journal for physics

Overcoming phonon-induced dephasing for indistinguishable photon sources

Tom Close[1], **Erik M Gauger**[1,2] **and Brendon W Lovett**[1,3,4]
[1] Department of Materials, Oxford University, Oxford OX1 3PH, UK
[2] Centre for Quantum Technologies, National University of Singapore, 3 Science Drive 2, Singapore 117543, Singapore
[3] SUPA, School of Engineering and Physical Sciences, Heriot Watt University, Edinburgh EH14 4AS, UK
E-mail: b.lovett@hw.ac.uk

New Journal of Physics **14** (2012) 113004 (17pp)
Received 25 June 2012
Published 7 November 2012
Online at http://www.njp.org/
doi:10.1088/1367-2630/14/11/113004

Abstract. Reliable single photon sources constitute the basis of schemes for quantum communication and measurement based quantum computing. Solid state single photon sources based on quantum dots are convenient and versatile but the electronic transitions that generate the photons are subject to interactions with lattice vibrations. Using a microscopic model of electron–phonon interactions and a quantum master equation, we here examine phonon-induced decoherence and assess its impact on the rate of production, and indistinguishability, of single photons emitted from an optically driven quantum dot system. We find that, above a certain threshold of desired indistinguishability, it is possible to mitigate the deleterious effects of phonons by exploiting a three-level Raman process for photon production.

[4] Author to whom any correspondence should be addressed.

Contents

1. Introduction

Single photon sources are an essential component of many quantum information processing (QIP) protocols, from quantum key distribution (QKD) protocols [1, 2] to linear optical quantum computing (LOQC) schemes [3–5]. Optical schemes using path erasure, a two-photon interference effect, can be used to generate long-range entanglement between physically separated systems [6–9]. Such procedures can be repeated on many different pairs of systems and so create a distributed cluster state [5, 10], which is the key resource required for implementation of measurement based quantum computing.

In order to be useful in these applications, a photon source must be of a high quality in two respects: it must reliably produce a single photon on demand, and the photons produced must be indistinguishable from one another.

To be perfectly indistinguishable, photons must have the same pulse width, bandwidth, polarization, arrival time at the detector and carrier frequency. Indistinguishability is vital if photons are to exhibit high quality quantum interference, and its consideration is therefore critical when designing photon sources for LOQC and path erasure entanglement generation. If photons can be distinguished even in principle, this can lead directly to imperfect LOQC gates, or to a lessening of the degree of entanglement generated in distributed cluster states. In QKD, indistinguishability is less important as interference effects are not required, but it is of paramount importance that no more than one photon is emitted on demand; multiple photon emission leads to security loopholes [5].

As a measure of indistinguishability we exploit the Hong–Ou–Mandel (HOM) effect [11], which relies on the bunching behaviour of identical photons when they are incident on a beam splitter with the same temporal profile. If the photons are indistinguishable, they will always emerge in and be detected in the same output arm (figure 1). The number of different-arm detection events are usually plotted as a function of arrival time of the two photons—and hence a 'dip' at a time difference of zero is an indicator of indistinguishability. The degree of distinguishability can be given by the HOM visibility, v_{HOM}, which is the proportion of same-arm detections, over many runs of the experiment. It is worth noting that this definition of v_{HOM} differs from the HOM dip commonly measured in experiments: the typical experimental setup involves continuously pumped systems, and looks for an absence of simultaneous detections in different detector arms; we consider an on-demand photon pair, and look at the probability that the two detections are in the same arm *over the complete run of the experiment*.

As mentioned above, besides indistinguishability, an essential characteristic of a good photon source is that it will consistently produce a single photon, but never more than one,

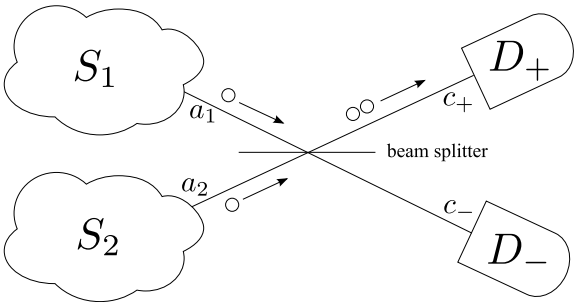

Figure 1. HOM effect: a pair of photons from two sources S_1 and S_2 incident on a beam splitter exhibit perfect bunching behaviour if they are completely indistinguishable. In this case the detectors D_+ and D_- will never click simultaneously.

on demand [12]. A laser source can be attenuated so that it gives zero or single photons most of the time. However, photons from classical laser sources obey Poissonian statistics so that in order to keep the two-photon event rate low the probability of a single photon may become unworkably small for many applications. In addition to this, Poissonian sources are unsuitable for two-photon interference experiments since the rate of two-photon production from a single source is similar to that for a single photon from each source [5]. It is worth noting that perfect efficiency should never be a requirement in any realistic optical QIP scheme, as these must always be tolerant to photon loss within other parts of the apparatus. However, a good photon source must be reasonably efficient to be useful, and we should not be forced to trade efficiency for other desirable characteristics.

The use of low-dimensional quantum systems as single photon sources avoids the efficiency problems of Poissonian sources. Successful experimental implementations have been realized in a number of different systems, including atom–cavity schemes [13–16], quantum dots [17, 18] and diamond colour centres [19–21]. While the majority of the work has been focused on the efficient production of a single photon, recent experiments in nitrogen-vacancy centres [20, 21] and quantum dots [22, 23] have demonstrated two-photon interference effects from different sources, albeit sacrificing efficiency by filtering out undesired frequencies. It has been suggested that cavities could be used in these systems, to enhance the emission into the target mode, reducing the need for filtering [24].

In order to improve the characteristics of a photon source, it is not sufficient to simply consider the material parameters of the system being used: one should also consider the approach used to control the system. Perhaps the simplest strategy is to excite the system first optically, either coherently or incoherently, and wait for the system to relax into its ground state, emitting a photon in the process; we will henceforth refer to this as the 'pulse–relax' technique. This approach makes minimal resource demands on the system and, due to its simplicity, is the technique proposed in some remote entanglement generation schemes [6, 8]. The pulse–relax approach is problematic in systems where the excited state is sensitive to decoherence, which will degrade the photon's indistinguishability [6, 25–27]. These effects can be reduced, for example by exploiting the Purcell effect to enhance the emission rate into the desired photon mode [28, 29] or by using temporal post-selection of emitted photons [27]. However, with experimental limits on cavity couplings both of these inevitably lead to lower efficiency as the proportion of emissions utilized falls [30].

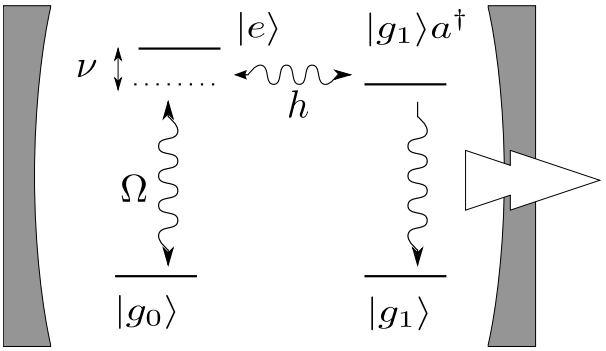

Figure 2. Effective level structure of a driven Λ-system inside an optical cavity. Here, Ω is the amplitude of an external (laser) driving field, h the optical dipole–cavity-coupling, and ν the shared detuning of the laser and the cavity transition frequency from the excited state. The system can decay into state $|g_1\rangle$ and in doing so emit a photon into a well-defined external mode.

A fundamentally different approach is to use more elaborate quantum electrodynamics schemes to release a photon from the system in a controlled manner. In particular, single photon sources using a Raman approach have been analysed [25, 26] and experimentally realized [13]. The approach places more demands on the system, requiring a three-level system with a Λ-system configuration. Each arm is coupled to either a classical or a quantum light field; in figure 2 we show the situation when one arm is driven classically, with a coupling Ω, and the other arm is coupled to a cavity mode with strength h. By detuning both arms of the Λ-system by the same amount ν, population is transferred from one arm to the other, while suppressing population in the top state. Provided that the coupling strengths are small in comparison to the detuning, $\Omega \ll \nu$ and $h \ll \nu$, we induce an effective coupling between the two low-lying states, which causes oscillations with Rabi frequency $h\Omega/4\nu$. The population in the excited state remains small at all times, and so any decoherence that arises due to environmental coupling to this excited state may be reduced using this strategy. In particular, a common realization of a single photon source is a quantum dot, in which the excited state typically has a different charge configuration to the ground state. This causes local lattice distortions, which in turn locally alter the electronic bandgap, thus inducing a coupling to acoustic phonons [31, 32] that can act as a noise source.

In this paper, we provide a detailed and realistic analysis of the effects of the lattice vibrations for single photon emitters based on (self-assembled) semiconductor quantum dots. By comparing a standard pulse–relax approach with the aforementioned Raman technique, we find that the latter can offer considerable improvements in terms of both photon indistinguishability and source efficiency. Our results extend and complement a previous study [26] which considered generic pure dephasing noise. However, here we also show that the precise choice of control parameters is important if phonon-induced decoherence is to be successfully suppressed.

2. Our model

For convenience of notation we consider the Λ-system detailed in figure 2 for both the pulse–relax and the Raman approach. In both cases one arm of the system is coupled to the

cavity with detuning ν. In the Raman scheme, the other arm is driven with strength Ω by a laser with a matching detuning ν, and the system starts in state $|g_0\rangle$. By contrast, we model the pulse–relax approach by setting $\Omega = \nu = 0$ and starting in state $|e\rangle$, ignoring the details of the excitation process. The fact that we are neglecting the excitation step in this simplified picture will slightly favour the pulse–relax approach, but is largely justified on the assumption that the initial excitation process takes place quickly compared with other system dynamics. Our framework thus allows us to consider the pulse–relax approach as a special case of the master equation we will now derive for the Raman approach.

We split the Hamiltonian into contributions from the emitter system and cavity (sys), the driving laser (dr), the unperturbed phonon bath (ph) and interaction terms between the system and phonon bath (sys–ph), system and target external mode (sys–mod), and system and other exernal modes (sys–ext):

$$H = H_{\mathrm{sys}} + H_{\mathrm{dr}} + H_{\mathrm{ph}} + H_{\mathrm{sys-ph}} + H_{\mathrm{sys-mod}} + H_{\mathrm{sys-ext}}. \tag{1}$$

The $H_{\mathrm{sys-mod}}$ and $H_{\mathrm{sys-ext}}$ terms are well understood, and we will treat these by adding in the appropriate Lindblad terms to our final master equation. In the following, we shall describe the rest of these terms separately.

Using the standard Jaynes–Cummings Hamiltonian, the Λ-system coupled to a cavity mode with strength h and detuning ν from resonance can be described by the following Hamiltonian:

$$H_{\mathrm{sys}} = (\omega + \nu)\,|e\rangle\langle e| + \omega a^{\dagger}a + \frac{h}{2}\left(|g_1\rangle\langle e|a^{\dagger} + \mathrm{h.c.}\right), \tag{2}$$

where h.c. denotes the Hermitian conjugate. ω is the cavity mode frequency.

We can restrict ourselves to one or zero cavity photons since the Jaynes–Cummings model preserves excitation number and after photon emission we assume that the emitter system remains in state $|g_1\rangle$—i.e. we make the approximation that once a photon has escaped re-excitation does not occur—at least until an appropriate reset step (such as thermal relaxation), which we assume happens on a much longer timescale than the photon emission dynamics. This allows us to replace $|g_1\rangle a^{\dagger}$ with a new combined atom–photon state $|g_a\rangle$ and $a^{\dagger}a$ with $|g_a\rangle\langle g_a|$.

The term H_{dr} describes a laser driving the transition $|g_0\rangle \leftrightarrow |e\rangle$ with coupling strength Ω, and whose frequency is detuned from resonance by the same ν parameter, yielding

$$H_{\mathrm{dr}} = \Omega\cos(\omega t)\,(|e\rangle\langle g_0| + \mathrm{h.c.})\,. \tag{3}$$

In a frame rotating with frequency ω and after performing the rotating wave approximation, assuming that $\omega \gg \nu, h, \Omega$, we are left with

$$H_{\mathrm{sys}} + H_{\mathrm{dr}} = \nu|e\rangle\langle e| + \frac{1}{2}\left(h|g_a\rangle\langle e| + \Omega|e\rangle\langle g_0|\right) + \mathrm{h.c.}, \tag{4}$$

for the total system Hamiltonian.

We model the phonons as a bath of harmonic oscillators

$$H_{\mathrm{ph}} = \sum_q \omega_q b_q^{\dagger} b_q, \tag{5}$$

which couple to the exciton state $|e\rangle$ through the deformation coupling with coupling constants $f_q = D|q|$ in the usual way [32]:

$$H_{\mathrm{sys-ph}} = |e\rangle\langle e| \sum_q f_q \left(b_q^{\dagger} + b_q\right). \tag{6}$$

The effect of the phonon bath on a driven quantum dot can be described using a Lindblad master equation [33], where the Lindblad operators induce phonon-assisted transitions between the dressed system eigenstates [34]. Being analogous to [33, 34], it suffices to outline the derivation of the phonon master equation only briefly in the following. To derive the master equation we must first diagonalize the system Hamiltonian, $H_{\rm sys} + H_{\rm dr}$. We find that the eigenvalues are

$$\lambda_0 = 0, \qquad \lambda_\pm = \frac{\nu \pm \sqrt{\nu^2 + \Omega^2 + h^2}}{2}, \tag{7}$$

with corresponding eigenvectors

$$\begin{aligned} |\psi_0\rangle &= n_0 \left(h\,|g_0\rangle - \Omega\,|g_a\rangle\right), \\ |\psi_\pm\rangle &= n_\pm \left(\Omega\,|g_0\rangle + h\,|g_a\rangle + 2\lambda_\pm\,|e\rangle\right). \end{aligned} \tag{8}$$

n_0 and $n_\pm$ are appropriate normalization factors. We now make the Born and Markov approximations which lead to the master equation [35] in standard Lindblad form:

$$\dot{\rho} = \mathrm{i}\,[\rho, H] + D_{\rm ph}(\rho), \tag{9}$$

with the phonon dissipator given by

$$D_{\rm ph}(\rho) = J(\Lambda)\left[(N(\Lambda)+1)\,D\,[P_\Lambda]\,\rho + N(\Lambda) D[P_\Lambda^\dagger]\rho\right], \tag{10}$$

where $D[L]\rho = L\rho L^\dagger - 1/2(L^\dagger L\rho + \rho L^\dagger L)$, $\Lambda = \lambda_+ - \lambda_-$ and $P_\Lambda = -|\psi_-\rangle\langle\psi_+|$. Note that the phonons only induce transitions between the two optically bright system eigenstates and do not couple to the dark $|\psi_0\rangle$. In the above equation $N(\Lambda)$ is the bosonic mode occupation number:

$$N(\omega) = \frac{1}{\mathrm{e}^{\beta\omega} - 1}, \tag{11}$$

$\beta = (k_{\rm B}T)^{-1}$ and we shall henceforth consider all systems at room temperature, $T = 298$ K. The spectral density function $J(\omega)$ represents the electron–phonon coupling weighted by the density of phonon modes [35]. We expect this to be dominated by deformation potential coupling, and in this case we obtain [33]:

$$J(\omega) = \alpha\omega^3\,\mathrm{e}^{-\left(\frac{\omega}{\omega_{\rm c}}\right)^2}. \tag{12}$$

We take $\alpha = 0.0027\,\mathrm{ps}^{-1}$ and $\omega_{\rm c} = 2.2\,\mathrm{ps}^{-1}$, values that agree well with experiments on self-assembled quantum dots [31, 36].

We absorb the rates in equation (10) into the Lindblad operators to obtain following decoherence operators:

$$U_+ = \sqrt{J(N+1)}|\psi_-\rangle\langle\psi_+|, \tag{13}$$

$$U_- = \sqrt{JN}|\psi_+\rangle\langle\psi_-|, \tag{14}$$

where we have taken $J = J(\Lambda)$ and $N = N(\Lambda)$. Note that if non-Markovian dynamics are taken into account [37] this can lead to effects on the ultra-short timescale, but these are in general much shorter than typical dynamics studied here.

As a measure of the degree of indistinguishability of the photons produced in the emission process, we consider the HOM visibility, which is the normalized probability of same-arm

detections obtained over many runs of the experiment,

$$v_{\mathrm{HOM}} = \frac{p_{\mathrm{same}} - p_{\mathrm{diff}}}{p_{\mathrm{same}} + p_{\mathrm{diff}}}, \tag{15}$$

where $p_{\mathrm{same}} = p(D_+ \cap D_+) + p(D_- \cap D_-)$ and $p_{\mathrm{diff}} = p(D_+ \cap D_-) + p(D_- \cap D_+)$, with $p(D_x \cap D_y)$ being the probability of obtaining a click in detector D_y followed by a click in detector D_x.

In order to calculate v_{HOM} we thus need to consider photons emitted from two copies of the system S_1 and S_2, one for each input arm of the beam splitter interferometer. The joint state of the system then inhabits the space $S = S_1 \otimes S_2$ (figure 1). We label the two cavity modes using annihilation operators a_1 and a_2. Using the input–output formalism (e.g. [38]) and neglecting incoming light, we can describe the modes outside the cavities as $a_{i,\mathrm{out}} = \sqrt{\kappa}$, where κ is the cavity leakage rate. The modes corresponding to detection in $D_\pm$ are labelled $c_\pm$ respectively. Due to the transformation performed by the beam splitter, $c_\pm$ can be written in terms of a_1 and a_2 as follows:

$$c_+ = \sqrt{\kappa}\frac{1}{\sqrt{2}}(a_1 + a_2)\,, \tag{16}$$

$$c_- = \sqrt{\kappa}\frac{1}{\sqrt{2}}(a_1 - a_2)\,. \tag{17}$$

We assume that the field in the mode outside the cavity is directly related to the field inside, neglecting the process of escape from the cavity. The effect on the system $S = S_1 \otimes S_2$ of a detection in the plus or minus output mode is then described by the projection operators

$$C_\pm = |g_1\rangle\langle g_a| \otimes \mathbb{I} \pm \mathbb{I} \otimes |g_1\rangle\langle g_a|. \tag{18}$$

We could now simulate many trajectories of this system and build up an estimate of v_{HOM} by averaging these [39]. Instead we use a semi-quantum master equation technique described in more detail in appendix. This allows us to find v_{HOM} in a single run of a master equation acting on a slightly larger Hilbert space.

When calculating v_{HOM} we must consider events in which photons trigger either detector, and events in which photons are spontaneously emitted into the environment. We introduce a set of process-states to record and labels these event classes (figure 3):

$$S_{\mathrm{P}} = \{P_0,\, P_+,\, P_-,\, P_{\mathrm{S}},\, P_{\mathrm{D}},\, P_{\mathrm{E}}\}\,. \tag{19}$$

The process-state starts as P_0 and remains there until an event of interest occurs. $P_{+/-}$ represents the process-state after a single photon has been detected in the $D_{+/-}$ detectors, respectively. After a second photon has been detected the process-state becomes $P_{\mathrm{S/D}}$, depending on whether the second photon was detected in the same or a different detector than the first. If at any point a photon is emitted into the environment the process moves to state P_{E}. When calculating the indistinguishability we can then ignore any population in state P_{E}, but we must include it when considering the overall efficiency of the process.

We must also identify the operators that cause the movement between the process-states. Before doing this we extend the state-space S of the system to include the process-states:

$$S = S_1 \otimes S_2 \otimes S_{\mathrm{P}}. \tag{20}$$

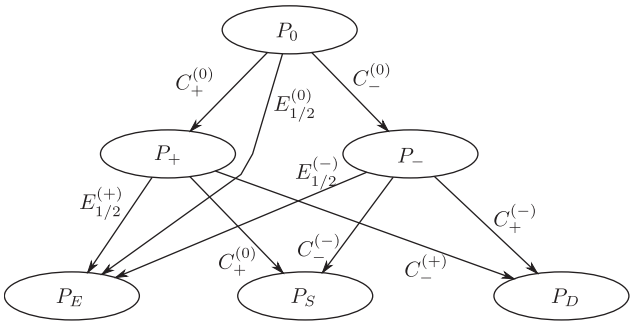

Figure 3. The system jump-space: on the first jump the system moves to P_+/P_-, depending on which arm the photon is detected in. After the second jump the system moves to state P_S/P_D, depending on whether the second photon was detected in the same or a different arm to the first. At any point the system can undesirably spontaneously emit into the environment, moving to the junk state P_E.

The detection operators are then given by

$$C_+^{(0)} = C_+ \otimes |P_+\rangle\langle P_0|, \tag{21}$$

$$C_+^{(+)} = C_+ \otimes |P_S\rangle\langle P_+|, \tag{22}$$

$$C_+^{(-)} = C_+ \otimes |P_D\rangle\langle P_-|, \tag{23}$$

$$C_-^{(0)} = C_- \otimes |P_-\rangle\langle P_0|, \tag{24}$$

$$C_-^{(-)} = C_- \otimes |P_S\rangle\langle P_-|, \tag{25}$$

$$C_-^{(+)} = C_- \otimes |P_D\rangle\langle P_+|, \tag{26}$$

where for example $C_+^{(-)}$ is the jump operator representing a second detection in the D_+ detector, when the first detection was in D_-. The spontaneous emission operators are given similarly:

$$E_1^{(0)} = |g_1\rangle\langle e| \otimes \mathbb{I}_S \otimes |P_E\rangle\langle P_0|, \tag{27}$$

$$E_2^{(0)} = \mathbb{I}_S \otimes |g_1\rangle\langle e| \otimes |P_E\rangle\langle P_0|, \tag{28}$$

$$E_1^{(+)} = |g_1\rangle\langle e| \otimes \mathbb{I}_S \otimes |P_E\rangle\langle P_+|, \tag{29}$$

$$E_2^{(+)} = \mathbb{I}_S \otimes |g_1\rangle\langle e| \otimes |P_E\rangle\langle P_+|, \tag{30}$$

$$E_1^{(-)} = |g_1\rangle\langle e| \otimes \mathbb{I}_S \otimes |P_E\rangle\langle P_-|, \tag{31}$$

$$E_2^{(-)} = \mathbb{I}_S \otimes |g_1\rangle\langle e| \otimes |P_E\rangle\langle P_-|, \tag{32}$$

where here $E_1^{(+)}$ represents a emission from S_1 acting after the first photon was detected in the D_+ detector.

Finally, we must modify our phonon decoherence operators. The subspaces corresponding to different process-states are classically separated by observable events. These classically

separated branches cannot exhibit interference, and we can therefore take the decoherence processes to occur independently on each branch:

$$U_{+,1}^{(0)} = \sqrt{J(N+1)}|\psi_-\rangle\langle\psi_+| \otimes \mathbb{I}_S \otimes |P_0\rangle\langle P_0|, \tag{33}$$

$$U_{-,1}^{(0)} = \sqrt{JN}|\psi_+\rangle\langle\psi_-| \otimes \mathbb{I}_S \otimes |P_0\rangle\langle P_0|, \tag{34}$$

$$U_{+,1}^{(+)} = \sqrt{J(N+1)}|\psi_-\rangle\langle\psi_+| \otimes \mathbb{I}_S \otimes |P_+\rangle\langle P_+|, \tag{35}$$

$$U_{-,1}^{(+)} = \sqrt{JN}|\psi_+\rangle\langle\psi_-| \otimes \mathbb{I}_S \otimes |P_+\rangle\langle P_+|, \tag{36}$$

$$U_{+,1}^{(-)} = \sqrt{J(N+1)}|\psi_-\rangle\langle\psi_+| \otimes \mathbb{I}_S \otimes |P_-\rangle\langle P_-|, \tag{37}$$

$$U_{-,1}^{(-)} = \sqrt{JN}|\psi_+\rangle\langle\psi_-| \otimes \mathbb{I}_S \otimes |P_-\rangle\langle P_-|, \tag{38}$$

with similar operators acting on the second system. We do not need decoherence operators acting on the P_S, P_D or P_E, since we are only concerned with populations in, and not coherences between, these states. Moreover, we only really need to keep track of the total population in each of these subspaces, and not the populations of each state that make up each subspace—a fact that we exploit to reduce the dimension of our problem for the numerical simulations.

We form a Lindblad master equation using these 24 Lindblad operators:

$$\dot{\rho} = \mathrm{i}\,[\rho, H] + \sum_i \gamma_i \left(L_i \rho L_i^\dagger - 1/2(L_i^\dagger L_i \rho + \rho L_i^\dagger L_i) \right). \tag{39}$$

The γ_i are the rates for each process. As noted earlier for the $U_{\pm,i}^{(j)}$ this rate is 1, as the rates have been incorporated into the Lindblad operators. For the $C_\pm^{(i)}$ we need $\gamma = \kappa$, the cavity leakage rate, which we take to be $3h$, a choice that allows for a reasonable enhancement of photon emission from the emitter system into the desired mode outside of the cavity, while preventing cavity photons being reabsorbed by the emitter system. For the $E_i^{(j)}$ we take $\gamma = 0.005\,\mathrm{ps}^{-1}$, assuming a radiative lifetime of 200 ps. Our model allows only for spontaneous emission directly from the excited state $|e\rangle$; we assume that there is no loss from the cavity to modes other than the target waveguide mode, and that all photons that are emitted into the target mode are detected. For similar cavities we expect these effects to impact the two approaches to equal extent.

The dimension of this extended space S is $4 \times 4 \times 6 = 96$. In fact we can reduce this by eliminating some unnecessary states from the subspaces. By carefully considering the basis states accessible in each the subspace corresponding to each process, we can reduce the number of system states to $9+6+6+1+1+1 = 24$. For our simulation we will need to calculate the density matrix for this system. As noted in the appendix, no coherences can exist between the different process-state subspaces. This reduces the number of density matrix elements we need to track to $9^2+6^2+6^2+1+1+1 = 116$.

3. Results

Figure 4 shows the HOM visibility obtained from, and spectral density used in, simulations of the pulse–relax technique. At low coupling strengths the phonon spectral density is small, and so phonon decoherence is largely avoided, giving high indistinguishability. As described earlier,

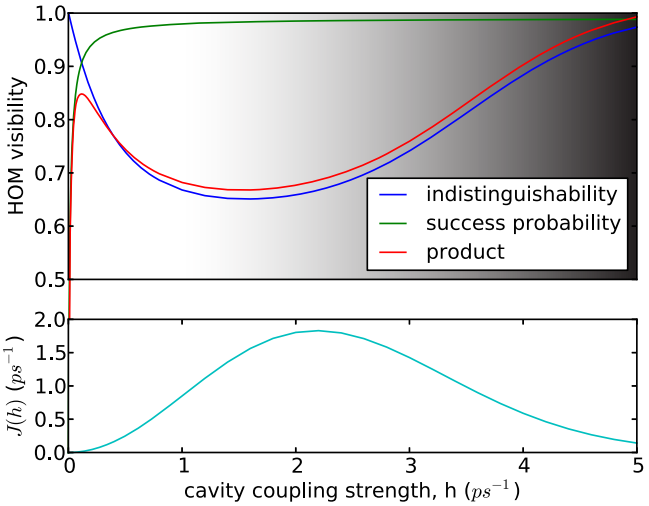

Figure 4. Pulse–relax technique: calculations are performed as a function of the cavity coupling strength. Upper panel: at realistic coupling strengths ($h < 1$) increased HOM indistinguishability necessarily entails a decrease in efficiency (success probability), with the product of the two (red curve) approaching zero. Here the spontaneous emission rate is $\Gamma = 0.005\,\mathrm{ps}^{-1}$. For overcoming phonon-induced decoherence and achieving a high success probability, we must move into a region of unrealistically high h, represented by the increasing level of shading of this plot. The lower panel shows the phonon spectral density, equation (12), evaluated at the cavity coupling strength h, giving a rate that is directly proportional to phonon-induced dephasing during the pulse–relax process.

we have fixed κ, the cavity leakage rate, to be $3\,h$, so the effective coupling to the target mode is proportional to the Purcell factor $h^2/\kappa \sim h$. This means that, for small h, the rate of photon emission into the cavity mode is slow and thus spontaneous emission into environmental optical modes is a problem. To take account of this effect, we define the 'combined HOM visibility', which is the product of success probability and bare HOM visibility, which approaches zero as $h \to 0$. Taking large coupling strengths allows one to access the region to the higher frequency side of the hump in the phonon spectral density and so avoid this problem, but is unrealistic given the cavity parameters currently obtainable experimentally. In the experimentally feasible region ($h < 1$) [40] we must therefore trade indistinguishability for efficiency.

In contrast, the Raman procedure (figure 5) avoids this trade-off. For small detuning the visibility is low, but this is because we do not get a proper Raman ground state transition unless $\nu \gg h$. If this condition is not met, the system simply undergoes a non-optimal detuned pulse–relax transition. Once we reach a detuning of around $\nu = 12h$ $(= 6\,\mathrm{ps}^{-1})$ the indistinguishability and efficiency both increase. Our choice of detuning size is limited in that it must be small in comparison with the original energy gap between the ground and excited states, and that it avoids any nearby excited states. This leaves us some freedom to use large detunings to push to frequencies above the region of high phonon spectral density. As the detuning is increased the efficiency saturates below unity. In this region both the time taken for the Raman

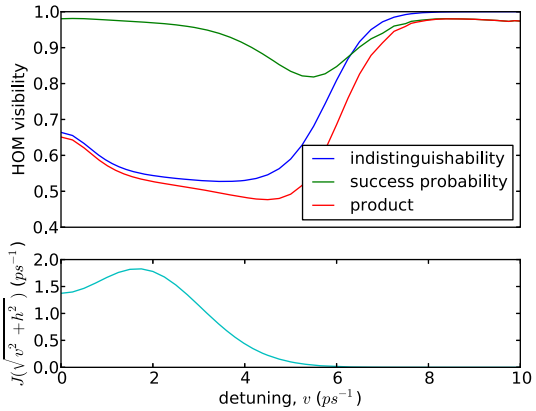

Figure 5. Raman technique, $h = 0.5$: by choosing a detuning to move beyond the region of high phonon spectral density we can achieve near-perfect indistinguishability. The efficiency in this region is high enough for a feasible photon source.

process and the average excited state population scale with the detuning squared, the two effects cancelling one another.

In many applications where photons are used, the product of efficiency and indistinguishability may not be the most useful metric for characterizing the performance of the source; often photon escape errors can be accounted for, and the indistinguishability of photons that are detected is the important figure of merit. We therefore also calculate the rate of production of pairs of photons of a given indistinguishability using each approach (figure 6). For our production rate we take

$$r_f = \frac{e_f}{t_f}, \tag{40}$$

where e_f is the efficiency and t_f is the time taken for 99% of the runs to have completed (possibly unsuccessfully), for parameters (h in the pulse–relax scheme, and v in the Raman scheme) chosen to obtain a given indistinguishability, f. This figure is somewhat approximate as it takes no account of how successful runs (where two photons are emitted into the correct modes) and unsuccessful runs are distributed within the process run time, and no allowance is made for time taken to reset the system in the event of a failure. The effect of the former is minor since in our model spontaneous emission can occur uniformly at any point of the process. We will revisit the effect of the latter shortly.

Even in the absence of spontaneous emission (figure 6, upper panel), the Raman procedure is quicker than the pulse–relax process at generating photons of a sufficiently high level of indistinguishability. With the dephasing parameters chosen in our model this occurs for indistinguishability of greater than 99.9%. In our model, spontaneous emission is the only process degrading the efficiency—without it we have perfect efficiency and so neither of the potential shortcomings discussed in the previous paragraph apply.

When spontaneous emission is added, we see a similar pattern but the indistinguishability threshold is very slightly lower. This is an upper bound, as here the reset time becomes important. The efficiency of the Raman procedure remains fixed at about 80%, requiring on average 1.25 runs per pair. In contrast, the efficiency of the pulse–relax procedure heads towards

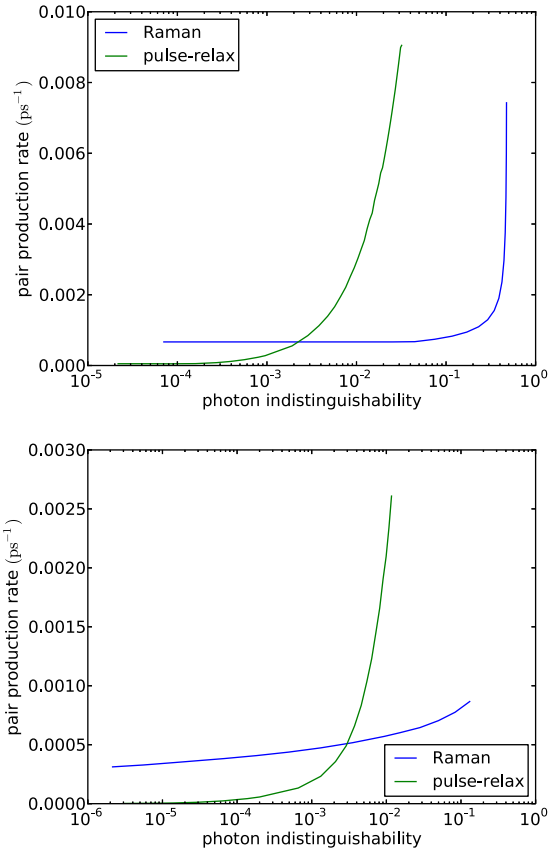

Figure 6. Rate of photon pair production: with no spontaneous emission (upper), and spontaneous emission with an excited-state lifetime of 200 ps (lower).

zero, meaning that many attempts will be needed to produce a pair. If the time taken to reset the system (to the excited state $|e\rangle$ in which we have assumed the pulse–relax system starts) is large, the Raman procedure will become advantageous at a far lower threshold.

4. Conclusion

To conclude, we have developed a realistic and microscopically justified model of the impact of phonons on solid state single photon sources. We used a modified, 'semi-quantum', master equation method for the efficient calculation of coincidence rates, without having to resort to a quantum Monte-Carlo simulation approach.

Our physical results are best summarized by considering the following scenario. Suppose you are working with a system where phonon dephasing and spontaneous emission are the dominant loss channels, where you have some control over the cavity parameters (h and κ), and that you are tasked with building a high indistinguisability, efficient, on-demand photon source. In this scenario, we find that a Raman technique is preferable to the pulse–relax approach. In particular, in addition to producing superior production rates at a given indistiguishability, the Raman approach we have taken only requires varying of the detuning—by tuning the cavity mode, and driving field—while leaving the other cavity properties fixed. This is in contrast to

the pulse–relax approach that we used for comparison, where we allowed the cavity coupling strength itself to be varied within a realistic range of values.

Acknowledgments

We thank Ahsan Nazir, Simon Benjamin, Pieter Kok, Alexia Auffèves, and Sean Barrett for useful discussions. This work was supported by the Engineering and Physical Sciences Research Council, UK and the National Research Foundation and Ministry of Education, Singapore. BWL thanks the Royal Society for a University Research Fellowship.

Appendix. Semi-quantum master equations

We are often interested in 'observable events' in quantum systems, such as the emission of a photon. When an event is observed the system undergoes a transition due to wave function collapse. During a period when no event is observed the system evolves according to a conditional master equation, reflecting the fact if events could be observed but are not, then this also informs our knowledge of the state. In order to answer questions about the probabilities and time distributions of events or chains of events, one approach is to use a quantum jump master equation to generate individual trajectories of the system. In each timestep we decide probabilistically whether an event should occur. If it does occur then the system collapses according to a quantum jump; if it does not occur then the system evolves conditioned on no jump occurring. Statistics about the quantities of interest are built up as many trajectories are created.

Here we look at a different approach to calculating the quantities relating to events that occur in such systems. Instead of simulating multiple trajectories of the system, we efficiently increase the size of the statespace to record the information of interest. This allows us to calculate the desired system properties, and their time evolution, by solving a single master equation.

Consider a system that can exist in a number of different states. Let a movement between these states constitute an event, and assume that each kind of event happens at a given rate. Such a system is heavily reminiscent of a classical continuous time Markov chain (CTMC), which can be represented as a graph with the states as nodes and the edges events weighted by the transition rates (figure A.1). Given an initial state i in a chain of size n, we can calculate the probability that at a later time t the chain is in state j, by solving the rate equations—a set of n ordinary differential equations.

Quantum systems differ from classical continuous-time Markov chains due to quantum superposition. We are not able to simply record the population in each quantum state as inter-state coherences are also important. Using a Markov chain to model the whole quantum system is not possible by definition—systems that can be modelled in this way do not exhibit quantum behaviour.

In what follows, it is helpful to explain carefully what we mean by 'state'. In quantum systems a state is usually a vector in the Hilbert space of the system. We shall call this a quantum-state. We can also refer to the 'state' of the overall process, considering for example a system that has emitted a photon to be in a different process-state to one which has not. A system changes process-state when an event is observed.

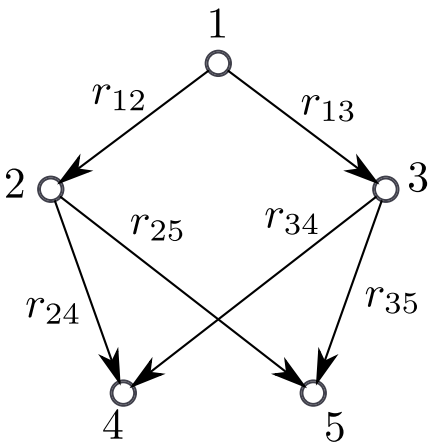

Figure A.1. A classical continuous-time Markov chain, with statespace $W = \{1, 2, 3, 4, 5\}$. The edge weight, r_{ij}, represents the transition rate from state i to state j. If $\rho_i(t)$ is the population in state i at time t, the system is governed by the rate equations $\dot{\rho}_i = \sum_{j \in W} r_{ji} \rho_j$.

Whereas thinking in terms of the CTMC is not useful when considering quantum-states, it is an effective way to think about process-states. As process-states are separated by an observed event, no coherences can exist between the two histories, making a CTMC approach feasible. Of course, process-states alone are not enough to model the whole system. Each process-state needs its own copy of the system attached to it. We can think of a Markov chain with a copy of our system at each node, where the transition rates are determined by the jump Lindblad operators corresponding to the events. Another way of thinking about this is that we extend our overall space with a set of process-states, to allow us to record events in the system.

Formally, we take a set of process-states S_{P}, transitions between which correspond to our observable jump events described by jump operators $J_{\mathrm{Q}}^{(i)}$. We extend the Hilbert space of our quantum system S_{Q} by forming the tensor product:

$$S = S_{\mathrm{Q}} \otimes S_{\mathrm{P}}. \tag{A.1}$$

The new Hamiltonian is given by

$$H = H_{\mathrm{Q}} \otimes \mathbb{I}. \tag{A.2}$$

If event $J_{\mathrm{Q}}^{(i)}$ causes a transition from system state a to b we say it is of type (a, b). Its action on the extended system S is described by

$$J^{(i)} = J_{\mathrm{Q}}^{(i)} \otimes |b\rangle\langle a|. \tag{A.3}$$

For any other Lindblad operators acting on the system $L_{\mathrm{Q}}^{(i)}$, we need to create a set of size $|S_{\mathrm{P}}|$ Lindblad operators—one to operate on each subspace independently:

$$s(L_{\mathrm{Q}}^{(i)}) = \left\{ L_{\mathrm{Q}}^{(i)} \otimes |j\rangle\langle j|,\ j \in S_{\mathrm{P}} \right\}. \tag{A.4}$$

At first glance it might appear that we have increased a system of size $m = |S|$ to size mn, where $n = |S_{\mathrm{P}}|$. While this is true, the situation is not as bad as it seems at first, because the coherences between the different subsystems are unimportant—instead of a density matrix of size $(nm)^2$ we can use a system of size nm^2, an increase linear in the number of system states.

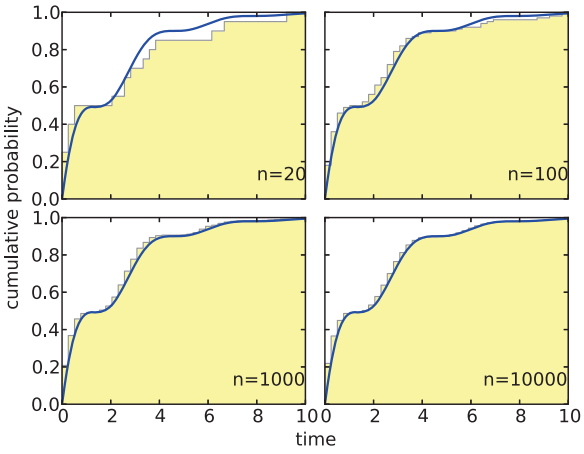

Figure A.2. Comparison of semi-quantum master equation approach with Monte Carlo simulations of $n = 20$, 100, 1000 and 10 000 runs, for the system described by equations (A.7)–(A.10). For the cumulative histogram plots we used horizontal binning with 40 bins, which explains why the horizontal resolution does not improve further for the larger values of n.

In practice we can often do better than this by eliminating unnecessary states from some of the subsystems.

As a simple concrete example, consider a resonantly driven two-level system $S_Q = \{|g\rangle, |e\rangle\}$, with Hamiltonian

$$H_Q = \Omega\left(|g\rangle\langle e| + |e\rangle\langle g|\right). \tag{A.5}$$

Suppose that it is also possible for the system to spontaneously emit from state $|e\rangle$ into the environment - a transition described by the jump operator

$$J_Q = |g\rangle\langle e|. \tag{A.6}$$

We are interested in knowing about the time distribution of the first time a photon is emitted. We add the two process-states 0 and 1, indicating whether the event has occurred or not. Our new system is described by:

$$S = \{|g0\rangle, |e0\rangle, |g1\rangle, |e1\rangle\}, \tag{A.7}$$

$$H = \Omega\left(|g0\rangle\langle e0| + |e0\rangle\langle g0| + |g1\rangle\langle e1| + |e1\rangle\langle g1|\right), \tag{A.8}$$

$$J_1 = |g1\rangle\langle e0|, \tag{A.9}$$

$$J_2 = |g1\rangle\langle e1|. \tag{A.10}$$

The population in the 1 subspace at time t will give us the probability a photon has been emitted by this time.

If we only cared about this distribution, we could reduce the size of the system by replacing the states $|g1\rangle$ and $|e1\rangle$ with a single state $|1\rangle$ to keep track of the cumulative jump probability over time. We would need to remove the last two terms from the Hamiltonian as well as J_2, and set $J_1 = |1\rangle\langle e0|$. Figure A.2 shows the cumulative jump probability for this system, showing agreement between the SQME results and Monte Carlo simulations with increasing numbers of runs.

References

[1] Bennett C H and Brassard G 1983 Quantum cryptography: public key distribution and coin tossing *Proc. IEEE Int. Conf. Comput. Syst. Signal Process.* pp 175–9

[2] Artur K Ekert 1991 Quantum cryptography based on Bell's theorem *Phys. Rev. Lett.* **67** 661–3

[3] Knill E, Laflamme R and Milburn G J 2001 A scheme for efficient quantum computation with linear optics *Nature* **409** 46–52

[4] Kok P, Munro W J, Nemoto K, Ralph T C, Dowling J P and Milburn G J 2007 Linear optical quantum computing with photonic qubits *Rev. Mod. Phys.* **79** 797

[5] Kok P and Lovett B W 2010 *Introduction to Optical Quantum Information Processing* (Cambridge: Cambridge University Press)

[6] Barrett S D and Kok P 2005 Efficient high-fidelity quantum computation using matter qubits and linear optics *Phys. Rev.* A **71** 060310

[7] Bose S, Knight P L, Plenio M B and Vedral V 1999 Proposal for teleportation of an atomic state via cavity decay *Phys. Rev. Lett.* **83** 5158

[8] Simon C and Irvine W T M 2003 Robust long-distance entanglement and a loophole-free bell test with ions and photons *Phys. Rev. Lett.* **91** 110405

[9] Lim Y L, Beige A and Kwek L C 2005 Repeat-until-success quantum computing *Phys. Rev. Lett.* **95** 030505

[10] Raussendorf R and Briegel H J 2001 A one-way quantum computer *Phys. Rev. Lett.* **86** 5188

[11] Hong C K, Ou Z Y and Mandel L 1987 Measurement of subpicosecond time intervals between two photons by interference *Phys. Rev. Lett.* **59** 2044–6

[12] Lounis B and Orrit M 2005 Single photon sources *Rep. Prog. Phys.* **68** 1129

[13] Kuhn A, Hennrich M and Rempe G 2002 Deterministic single-photon source for distributed quantum networking *Phys. Rev. Lett.* **89** 067901

[14] McKeever J, Boca A, Boozer A D, Miller R, Buck J R, Kuzmich A and Kimble H J 2004 Deterministic generation of single photons from one atom trapped in a cavity *Science* **303** 1992–4

[15] Darquie B, Jones M P A, Dingjan J, Beugnon J, Bergamini S, Sortais Y, Messin G, Browaeys A and Grangier P 2005 Controlled single-photon emission from a single trapped two-level atom *Science* **309** 454–6

[16] Hijlkema M, Weber B, Specht H P, Webster S C, Kuhn A and Rempe G 2007 A single-photon server with just one atom *Nature Phys.* **3** 253–5

[17] Kako S, Santori C, Hoshino K, Gotzinger S, Yamamoto Y and Arakawa Y 2006 A gallium nitride single-photon source operating at 200 k *Nature Mater.* **5** 887–92

[18] Hennessy K, Badolato A, Winger M, Gerace D, Atature M, Gulde S, Falt S, Hu E L and Imamoglu A 2007 Quantum nature of a strongly coupled single quantum dot-cavity system *Nature* **445** 896–9

[19] Wu E, Rabeau J R, Roger G, Treussart F, Zeng H, Grangier P, Prawer S and Roch J-F 2007 Room temperature triggered single-photon source in the near infrared *New J. Phys.* **9** 434

[20] Bernien H, Childress L, Robledo L, Markham M, Twitchen D and Hanson R 2012 Two-photon quantum interference from separate nitrogen vacancy centers in diamond *Phys. Rev. Lett.* **108** 043604

[21] Sipahigil A, Goldman M L, Togan E, Chu Y, Markham M, Twitchen D J, Zibrov A S, Kubanek A and Lukin M D 2012 Quantum interference of single photons from remote nitrogen-vacancy centers in diamond *Phys. Rev. Lett.* **108** 143601

[22] Flagg E B, Muller A, Polyakov S V, Ling A, Migdall A and Solomon G S 2010 Interference of single photons from two separate semiconductor quantum dots *Phys. Rev. Lett.* **104** 137401

[23] Patel R B, Bennett A J, Farrer I, Nicoll C A, Ritchie D A and Shields A J 2010 Two-photon interference of the emission from electrically tunable remote quantum dots *Nature Photon* **4** 632–5

[24] Su C-H, Greentree A D and Hollenberg L C L 2008 Towards a picosecond transform-limited nitrogen-vacancy based single photon source *Opt. Express* **16** 6240–50

[25] Kiraz A, Atatüre M and Imamoğlu A 2004 Quantum-dot single-photon sources: prospects for applications in linear optics quantum-information processing *Phys. Rev.* A **69** 032305

[26] Santori C, Fattal D, Fu K-M C, Barclay P E and Beausoleil R G 2009 On the indistinguishability of Raman photons *New J. Phys.* **11** 123009
[27] Nazir A and Barrett S D 2009 Overcoming non-markovian dephasing in single-photon sources through postselection *Phys. Rev.* A **79** 011804
[28] Purcell E M 1946 Long lived coherence in self-assembled quantum dots *Phys. Rev.* **69** 681
[29] Englund D, Fattal D, Waks E, Solomon G, Zhang B, Nakaoka T, Arakawa Y, Yamamoto Y and Vučković J 2005 Controlling the spontaneous emission rate of single quantum dots in a two-dimensional photonic crystal *Phys. Rev. Lett.* **95** 013904
[30] Auffèves A, Gerace D, Gérard J-M, França Santos M, Andreani L C and Poizat J-P 2010 Controlling the dynamics of a coupled atom–cavity system by pure dephasing *Phys. Rev.* B **81** 245419
[31] Ramsay A J, Venu Gopal A, Gauger E M, Nazir A, Lovett B W, Fox A M and Skolnick M S 2010 Damping of exciton Rabi rotations by acoustic phonons in optically excited InGaAs/GaAs quantum dots *Phys. Rev. Lett.* **104** 017402
[32] Mahan G D 2000 *Many Particle Physics* (*Physics of Solids and Liquids*) 3rd edn (Berlin: Springer)
[33] Gauger E M, Benjamin S C, Nazir A and Lovett B W 2008 High-fidelity all-optical control of quantum dot spins: detailed study of the adiabatic approach *Phys. Rev.* B **77** 115322
[34] Gauger E M and Wabnig J 2010 Heat pumping with optically driven excitons *Phys. Rev.* B **82** 073301
[35] Breuer H P and Petruccione F 2002 *The Theory of Open Quantum Systems* (Oxford: Oxford University Press)
[36] Ramsay A J, Godden T, Boyle S J, Gauger E M, Nazir A, Lovett B W, Fox A M and Skolnick M S 2010 Phonon-induced Rabi-frequency renormalization of optically driven single InGaAs/GaAs quantum dots *Phys. Rev. Lett.* **105** 177402
[37] Kaer P, Lodahl P, Jauho A-P and Mork J 2012 Microscopic theory of indistinguishable single-photon emission from a quantum dot coupled to a cavity: the role of non-Markovian phonon-induced decoherence http://arxiv.org/abs/1203.6268
[38] Walls D F and Milburn G J 2008 *Quantum Optics* 2nd edn (Berlin: Springer)
[39] Tian L and Carmichael H J 1992 Quantum trajectory simulations of two-state behavior in an optical cavity containing one atom *Phys. Rev.* A **46** R6801–4
[40] Majumdar A, Englund D, Bajcsy M and Vučković J 2012 Nonlinear temporal dynamics of a strongly coupled quantum-dot cavity system *Phys. Rev.* A **85** 033802